mathematics

MDPI

Article

Introducing a Precise System for Determining Volume Percentages Independent of Scale Thickness and Type of Flow Regime

Abdulilah Mohammad Mayet [1], Seyed Mehdi Alizadeh [2], Zana Azeez Kakarash [3], Ali Awadh Al-Qahtani [1], Abdullah K. Alanazi [4], Hala H. Alhashimi [5], Ehsan Eftekhari-Zadeh [6,*] and Ehsan Nazemi [7]

1 Electrical Engineering Department, King Khalid University, Abha 61411, Saudi Arabia; amayet@kku.edu.sa (A.M.M.); alawalqahtani@kku.edu.sa (A.A.A.-Q.)
2 Petroleum Engineering Department, Australian College of Kuwait, West Mishref 13015, Kuwait; s.alizadeh@ack.edu.kw
3 Department of Information Technology, University of Human Development, Sulaymaniyah 07786, Iraq; zana.azeez@uhd.edu.iq
4 Department of Chemistry, Faculty of Science, Taif University, P.O. Box 11099, Taif 21944, Saudi Arabia; aalanaz4@tu.edu.sa
5 Department of Physics, College of Science, Imam Abdulrahman Bin Faisal University, P.O. Box 1982, Dammam 31441, Saudi Arabia; halhashim@iau.edu.sa
6 Institute of Optics and Quantum Electronics, Friedrich-Schiller-University Jena, Max-Wien-Platz 1, 07743 Jena, Germany
7 Imec-Vision Laboratory, Department of Physics, University of Antwerp, 2610 Antwerp, Belgium; ehsan.nazemi@uantwerpen.be
* Correspondence: e.eftekharizadeh@uni-jena.de

Abstract: When fluids flow into the pipes, the materials in them cause deposits to form inside the pipes over time, which is a threat to the efficiency of the equipment and their depreciation. In the present study, a method for detecting the volume percentage of two-phase flow by considering the presence of scale inside the test pipe is presented using artificial intelligence networks. The method is non-invasive and works in such a way that the detector located on one side of the pipe absorbs the photons that have passed through the other side of the pipe. These photons are emitted to the pipe by a dual source of the isotopes barium-133 and cesium-137. The Monte Carlo N Particle Code (MCNP) simulates the structure, and wavelet features are extracted from the data recorded by the detector. These features are considered Group methods of data handling (GMDH) inputs. A neural network is trained to determine the volume percentage with high accuracy independent of the thickness of the scale in the pipe. In this research, to implement a precise system for working in operating conditions, different conditions, including different flow regimes and different scale thickness values as well as different volume percentages, are simulated. The proposed system is able to determine the volume percentages with high accuracy, regardless of the type of flow regime and the amount of scale inside the pipe. The use of feature extraction techniques in the implementation of the proposed detection system not only reduces the number of detectors, reduces costs, and simplifies the system but also increases the accuracy to a good extent.

Keywords: pipeline's scale; feature extraction; GMDH neural network; two-phase flow

MSC: 68T01

Citation: Mayet, A.M.; Alizadeh, S.M.; Kakarash, Z.A.; Al-Qahtani, A.A.; Alanazi, A.K.; Alhashimi, H.H.; Eftekhari-Zadeh, E.; Nazemi, E. Introducing a Precise System for Determining Volume Percentages Independent of Scale Thickness and Type of Flow Regime. *Mathematics* **2022**, *10*, 1770. https://doi.org/10.3390/math10101770

Academic Editor: Jüri Majak

Received: 25 April 2022
Accepted: 20 May 2022
Published: 23 May 2022

1. Introduction

Gas volume fraction (GVF) is one of the important parameters in describing biphasic flows in the oil industry because calculating the empty fraction is necessary to predict values such as heat transfer, pressure drop, and critical two-phase flow occurrence to calculate the empty fraction. Quantitative knowledge of these parameters is required in the oil industry.

Various methods can be used to measure the empty fraction [1]. Although the main axis of diagnosis in this study is gamma radiation, hydrostatic, hydrometric, and ultrasonic are other useful alternative techniques for detecting the volume fraction of multiphase flow. In [2], an artificial neural network (ANN) and extraction of various features were used to increase the accuracy of two-phase flowmeters based on X-ray radiation. An X-ray tube for sending photons, a NaI detector for absorbing photons, and a Pyrex glass pipe through which the photons pass form the structure used in this paper. The Monte Carlo MCNP-X code was used to model the geometry. Feature extraction was performed in the time domain with five features and was given as input to the neural network. Multi-Layer Perceptron (MLP) was applied to approximate the function related to the output–input relationship. The procedure proposed by Basahal et al. was able to accurately obtain the flow pattern and predict the volume fraction of two-phase flow components. The root mean square error (*RMSE*) was less than 0.51, the mean absolute error (MAE) was less than 0.4, and the mean absolute error percentage (MAPE) was less than 1.16%. Taylan et al. [3] conducted related research and used a combination almost identical to the previous study. Their structure consists of a Pyrex glass pipe in the middle, an X-ray tube on one side, and two detectors on the other side. The difference was in the number of detectors. Flow regime and volume percentage in a three-phase flow of oil, water, and gas were calculated. As usual, the simulation procedure was performed by MCNP-X code. The signals were collected and the simulations were completed, then the Fast Fourier Transform (FFT) was used to convert to the frequency domain. The first and second dominant frequency amplitudes were used as neural network inputs. Three RBFNN networks were trained to predict the type of regime and the volume percentage of gas and water. Correct diagnosis of all flow regimes and determination of volume percentages with Mean Relative Error (*MRE*) less than 2.02% shows that the use of frequency features can be effective in determining these important parameters. The scale formation inside a few pipes can be seen in Figure 1. The proposed structure also includes two detectors, one that absorbs the transmitted photons and the other the scattered photons.

Figure 1. An example of scale deposition in few pipes.

Roshani and his colleagues in [4] attempted to use the obtained absorption spectra to train and test the multilayer perceptron network (MLP) using an X-ray source, a detector, and other routine procedures. After training, MLP neural networks can conjecture the volume ratio of each petroleum product with an average absolute error of 2.72. Sattari et al., in two studies [5,6], examined the time characteristics to determine the volume

percentages and the type of flow regimes. Research [5] extracted a large number of time-domain characteristics and identified the most effective ones in a creative way. In [6], time characteristics were considered the input of the GMDH neural network. Although the accuracy of the obtained networks was very high in these studies, not considering the scale thickness in the oil pipes was one of the weaknesses of these studies. In [7], GMDH neural networks were used to determine the volume percentages, but with the difference that the neural network inputs were features named count under Compton continuum, count under photopeak of 1.173 MeV, count under photopeak of 1.333 MeV, and the average value of the recorded spectrum. In other studies, signal frequency characteristics [8] and signal wavelet transform characteristics [9,10] were used to determine the volume percentages. The deposition of scale over time in oil pipelines is undeniable, which reduces the efficiency of oil industry systems and devices. Sedimentation of the scale inside the pipe causes non-invasive detection systems to fail to function properly. In all the mentioned studies, failure to investigate the effects of scale thickness on the detection of multiphase flow parameters can be introduced as a major shortcoming. In [11], a method of attenuation of gamma through a dual-energy source with an RBFNN neural network is proposed to determine the thickness of the scale formed in oil pipelines. Failure to extract the appropriate characteristics from the received signals and the use of raw signals as input to the neural network has not only imposed a large computational load on the system but has also prevented access to high accuracy. In research [12], although both the effects of scale thickness and frequency characteristics of signals were investigated, the lack of high accuracy in the detection system indicates the inadequacy of frequency characteristics in determining the type of flow regimes and predicting volume percentages. Inspired by previous research, this study attempted to measure the volume percentage under conditions where the scale was deposited inside the pipe. For this purpose, different conditions, including three different flow regimes in different volume percentages, as well as the number of different scales in the pipe, were simulated so that these different conditions can be considered as neural network inputs for training. Wavelet features were used to reduce computational costs and better interpret data as well as achieve high accuracy. Additionally, in this research, the number of volume percentages independent of the type of flow regime and the amount of scale inside the pipe can be identified with very high accuracy, which are the most important contributions of this research. The proposed method can be used in many fields of science, including medicine [13], chemical [14], and micro and nanofluidics [15,16], which can be the subject of future studies.

2. Simulation Setup

The modeling part of the detection system of this research was performed using version X of the Monte Carlo Particle Code (MCNPX) [17]. The mentioned diagnostic system is illustrated in Figure 2. There is a dual-source with a protective housing that directs gamma radiation to a pipe containing fluid at the top of the image. In the middle of the image is a pipe containing fluid, inside which a scale is also formed. At the bottom of the image, a detector was placed that absorbs photons passing through the pipe and collects the data. The attenuation for a narrow gamma-ray beam follows Lambert–Beer's law according to the following equation:

$$I = I_0 e^{-\mu \rho x} \tag{1}$$

where the intensity of uncollided and primary photons are shown by I and I_0, respectively. μ and ρ represent the mass attenuation coefficient and density of absorber material, respectively. x is the beam path length through the absorber

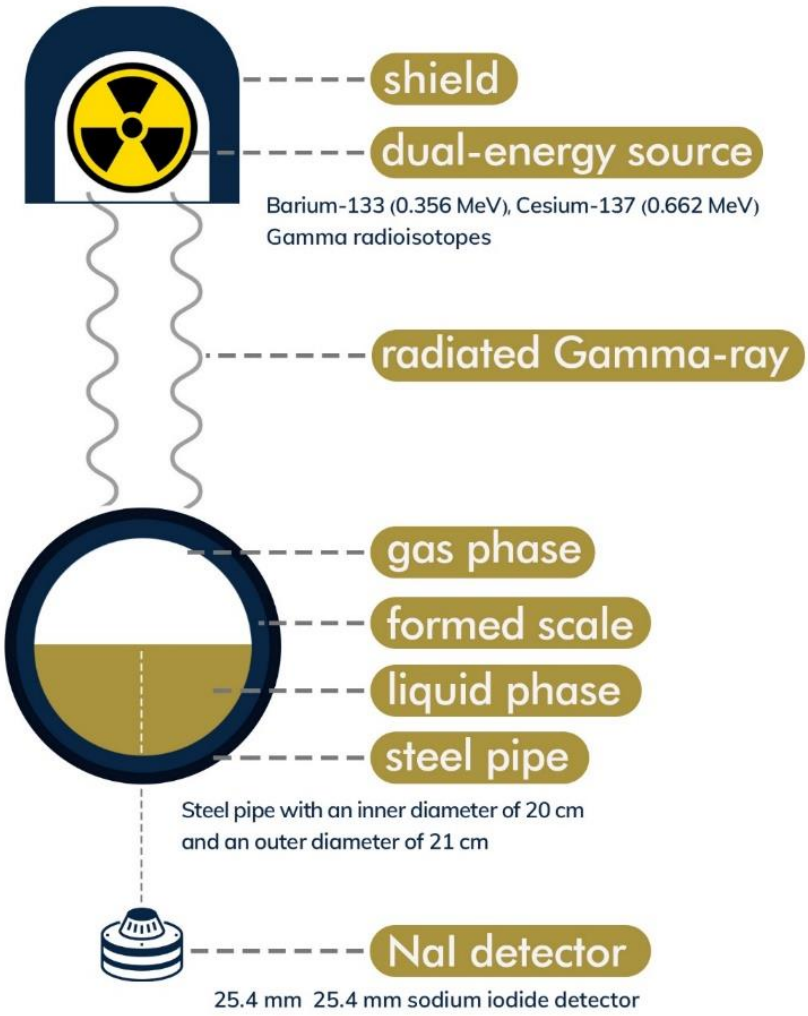

Figure 2. The detection system, respectively, from top to bottom: source shield, dual energy source, radiated gamma ray, gaseous phase, scale formed, liquid phase, steel pipe, NaI detector.

The energy source of the structure is a gamma source with two isotopes, cesium-137 and barium-133, the former operating at 0.662 MeV and the latter at 0.356 MeV. Three homogeneous, annular, and stratified flow regimes with steps of 15% in a volume percentage of 10% to 85% with seven various scale thicknesses (0 cm, 0.5 cm, 1 cm, 1.5 cm, 2 cm, 2.5 cm, and 3 cm) was simulated. Inside the pipe, there was a symmetrical layer of $BaSO_4$ with various thicknesses. In fact, the effects of changing the velocity, temperature, and pressure of each phase showed themselves in the type of flow regime formed inside the pipe [18,19]. For example, if the velocity of the gas phase inside the pipe is too high, it will cause the liquid phase to stick to the wall of the pipe, resulting in the formation of an annular phase. If in a horizontal pipe, the pressure of both phases is low and in the same range, due to the density difference between the two materials, the liquid phase is placed at the bottom of the pipe, and the gas phase is placed on top of it. This type of flow regime is called stratified. The recorded spectra for different scale thicknesses of 1 cm and different empty space fractions are shown in Figure 3. What was achieved in this study was confirmed by several experiments that were already performed in our previous articles [20]. The obtained detector responses were compared in experimental and simulation. Since the Tally output in the MCNP code is per source particle, both were normalized to units. The value of 2.2% for the detector response was the maximum relative difference between the simulation data and the experimental data. As can be seen, a good agreement was obtained between the experimental data and the simulation results. It is worth noting that the experiments and,

consequently, the simulations were performed in static conditions. The actual working conditions were dynamic, but the reference points for flowmeter training were fixed and could be considered static. In real conditions, multiphase flow meters were used to train flowmeters to determine the volume fraction and detect flow regimes. One of the cases in which rapid active gamma-ray neutron analysis was used for quantitative analysis for fast, non-intrusive, and online measurements of multiphase oil/gas/seawater flow is [21]. In the research that was conducted, although the simulations were used in real conditions, they were considered in static conditions. In [22], to describe the water extracted from offshore oil wells, the detection of transmitted and scattered gamma radiation was used, and its possibility was investigated. They determined the salinity and even the type of salt in the extracted water by measuring the gamma rays scattered, gamma rays transmitted, and calibration

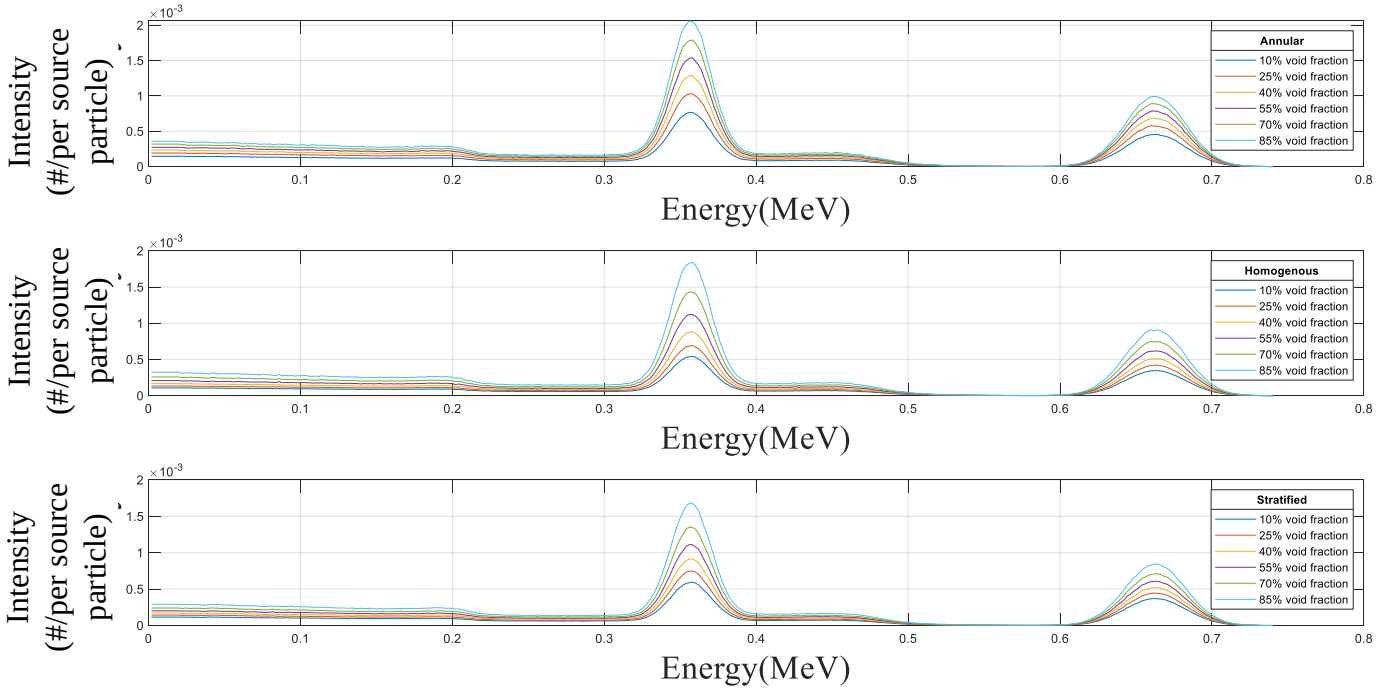

Figure 3. The recorded signal by the detector for all three simulated regimes at 1 cm scale thickness in different void fractions.

Figure 3 show the amount of energy received by the detector in terms of count per source particle. At two energies, 0.662 MeV and 0.356 MeV, this graph peaked, which is due to the energy of the dual-energy source of cesium-137 and barium-133. The rest of the spectrum received by the detector is due to the interaction of photons sent by the source with the environment, resulting in the loss of energy and ultimately received by the detector.

3. Discrete Wavelet Transform

The received signal can be broken down into several sets by discrete wavelet transform (DWT), and each set is a time series of coefficients that describe the temporal evolution of the signal in the corresponding frequency band. One of the most common methods of time-frequency filtering is the use of discrete wavelet transform (DWT) [23,24]. The multi-resolution analysis is possible by decomposing the discrete signal $x(n)$ into low and high-frequency components using the DWT method. An iterative Mallat algorithm is required to determine DWT. This method works based on a mother wavelet function and a corresponding scaling function to determine the high and low band filters. The

signal x (n) is decomposed into low aj, k (approximately) and high dj, k (in detail) frequency components (Figure 4) with multilevel filter banks:

$$a_{j,k} = \sum_l h(l - 2k)a_{j-1,m} \quad (2)$$

$$d_{j,k} = \sum_l g(l - 2k)a_{j-1,m} \quad (3)$$

where k is related to the translation at each level of the wavelet function. l is the number of levels and is an integer scale. j is a parameter that affects the DWT scaling. h (l) and g (l) are low-pass and high-pass quadrature filters, respectively. m is used in the scaling function as a translation of the j scale. Wavelet transform includes several families of wavelet functions such as Daubechies, Haar, and so on. The Daubechies 2 (db2) wavelet was selected to analyze the signals received from the scintillator detector.

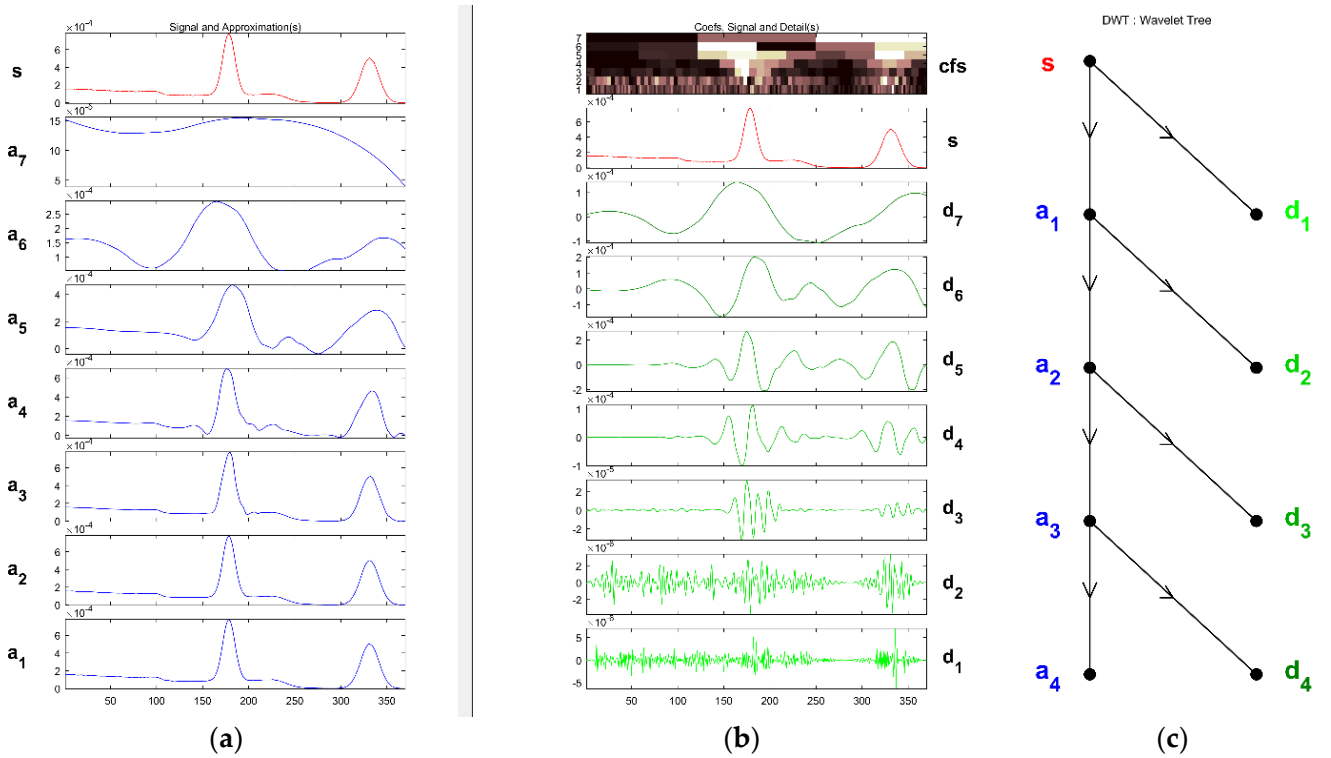

Figure 4. (**a**) Approximation signals, (**b**) detail signals, and (**c**) wavelet tree.

As can be seen in Figure 4, performing the wavelet transform operation from step 5 onwards no longer provides acceptable high-frequency information, so to reduce the computational volume, the wavelet operation is performed up to the fourth step. The approximation signals of step 4 (a4) and details of step 1 to 4 (d4, d3, d2, and d1) were averaged, and these characteristics were used as the input of the GMDH Neural Network for training.

4. Artificial Neural Network

In 1968, a Ukrainian mathematician developed a method for learning inductive statistics called the Group Method of Data Handling (GMDH), which later made him famous [25]. A self-control model was developed with the power to monitor the synthesis and related system problems and to solve predictions and classifications. It is worth mentioning that, in the recent years, various mathematical approaches have been used in different research fields such as electrical and computer engineering [26–30], mechanical engineering [31–34], civil and urban engineering [35–37], biomedical engineering [38,39], industrial engineering [40–43], and physics [44,45], but among them, ANN is the most well-known

and powerful numerical tool for prediction and classification [46–48]. Neuron values, invisible layer, effective input profile, and efficient network fabrication were determined independently in the GMDH operation. It is assumed that the input–output relationship of the system is characterized as a significant order polynomial, which is shown below as the Kolmogorov–Gabor polynomial.

$$y = a_0 + \sum_{i=1}^{m} a_i x_i + \sum_{i=1}^{m}\sum_{j=1}^{m} a_{ij} x_i x_j + \sum_{i=1}^{m}\sum_{j=1}^{m}\sum_{k=1}^{m} a_{ijk} x_i x_j x_k + \ldots \quad (4)$$

where a ($a_1, a_2, \ldots, a_m$) are weights or coefficients of vector, x ($x_1, x_2, \ldots, x_m$) are also vector inputs or the same extracted features, and y is the output of the network. The steps of the GMDH algorithm are as follows:

Step A: Generating novel variants $z_1, z_2, \ldots, z_{\binom{m}{2}}$. In this part, for the total non-dependent variables (characteristics) ($x_1, x_2, \ldots, x_m$), two synchronically and for any $\binom{m}{2}$ admixture, the quadratic regression polynomials are computed by considering Equation (5).

$$Z = c_1 + c_2 x_i + c_3 x_j + c_4 x_i^2 + c_5 x_j^2 + c_6 x_i x_j \quad (5)$$

This step aims to achieve the c_i coefficients. The least-squares algorithm was utilized to obtain the desired coefficients. Each obtaining $\binom{m}{2}$ compiled quadratic regression polynomial approximates the insignificant output.

Step B: Screening of non-significant z's in such a way that the error of each output in the given neurons (each neuron must approximate the quadratic regression polynomial) is calculated with the desired output, and the outputs (neurons) with the maximum error rates are not based on a scale of options. Another is applied to build the following layer. Here, the first latent layer is produced, and the affected neurons are systematically selected.

Step C: Applying modern variables ($z_1, z_2, \ldots, z_{\binom{m}{2}}$) as the quadratic regression polynomial inputs to generate modern variables. It means that the novel polynomial is obtained from a bygone polynomial ($z_1, z_2, \ldots, z_{\binom{m}{2}}$) by making polynomials of polynomials; the high-order polynomial was preserved, solving intricate and nonlinear issues. Then, step B was repeated, and the outputs were considered with the best estimate of the desired outputs. After the creation of hidden layer number 2, the production of new polynomials and their best approximations takes enough time to obtain the best input–output relationships and eventually to become Kolmogorov–Gabor polynomials.

Step D: Checking the GMDH neural network. At this stage, the evaluation of the final model against the experimental data set is performed to determine that the neural network has specifically determined the output–input relevance. In the present study, the sample percentage for GMDH neural network training is approximately 70% (88 samples), and the sample percentage for neural network testing is 30% (38 samples). The GMDH neural network training flowchart is shown in Figure 5.

To estimate the volume fraction of each phase in this investigation, a GMDH network was used, and the derived features (as discussed in the previous step) were considered as inputs of the GMDH neural network for testing and training.

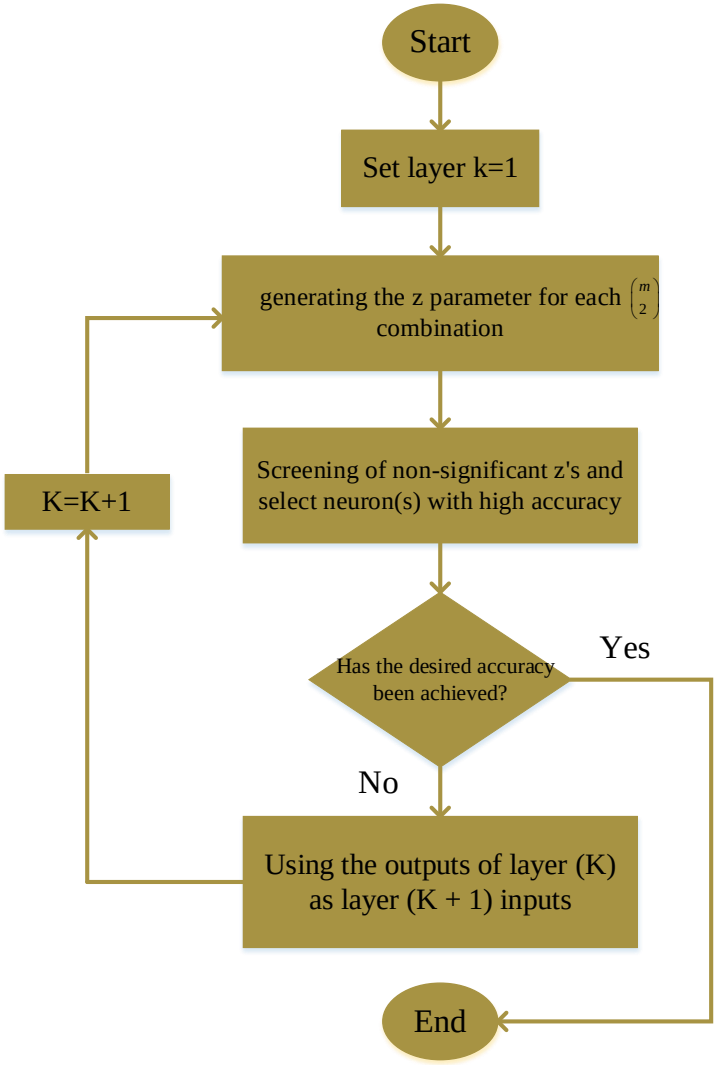

Figure 5. The GMDH neural network training flowchart.

5. Result and Discussion

In this research, a network structure of GMDH was taught with the mean signals of the fourth stage approximation and the mean signals of the details of the first to fourth stages of the wavelet transform. The output of this network is the percentage of empty volume in the pipe. The structure of this network is shown in Figure 6. To show the accuracy of the designed network, the regression diagram and the error diagram for both the training and test data sets can be seen in Figure 7. It should be noted that three error criteria with the names of mean relative error percentage (*MRE*%), mean square error (*MSE*), and root mean square error (*RMSE*) are calculated and shown in Table 1 to determine the accuracy of the network according to the following equations.

$$MRE\% = 100 \times \frac{1}{N} \sum_{j=1}^{N} \left| \frac{X_j(Exp) - X_j(Pred)}{X_j(Pred)} \right| \quad (6)$$

$$MSE = \frac{\sum_{j=1}^{N} \left(X_j(Exp) - X_j(Pred) \right)^2}{N} \quad (7)$$

$$RMSE = \left[\frac{\sum_{j=1}^{N} \left(X_j(Exp) - X_j(Pred) \right)^2}{N} \right]^{0.5} \quad (8)$$

where N is the number of data, 'X (*Exp*)' and 'X (*Pred*)' stands for the experimental and predicted (ANN) values, respectively.

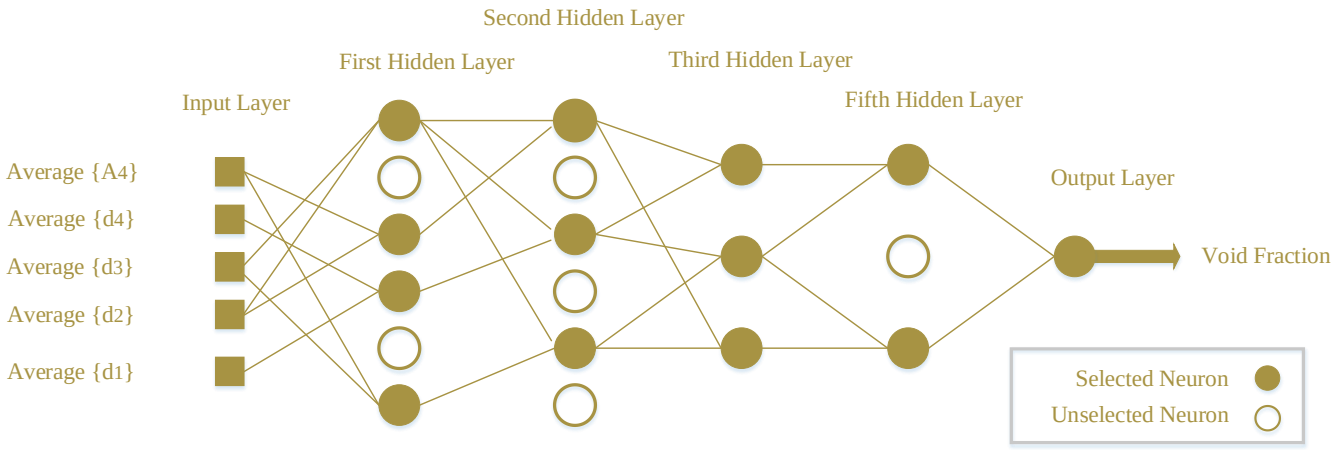

Figure 6. The structure of designed network.

Table 1. Calculated errors.

Data Set	*MRE*%	*MSE*	*RMSE*
Train	1.22	0.19	0.44
Test	0.97	0.12	0.35

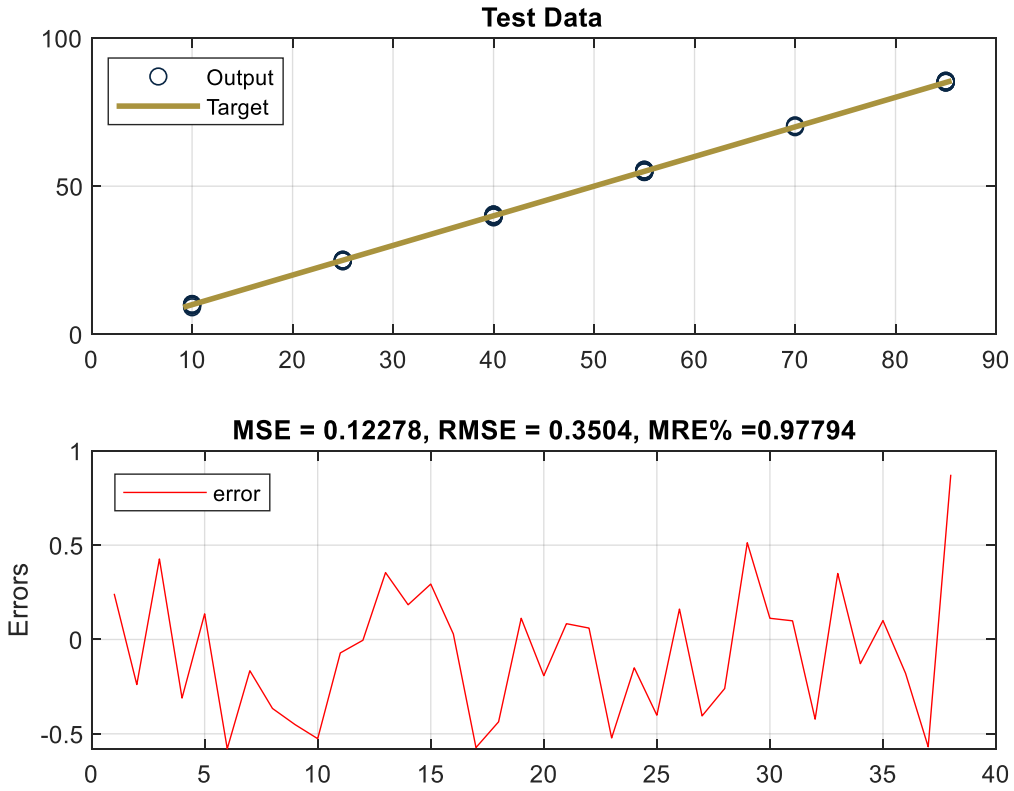

(a)

Figure 7. *Cont.*

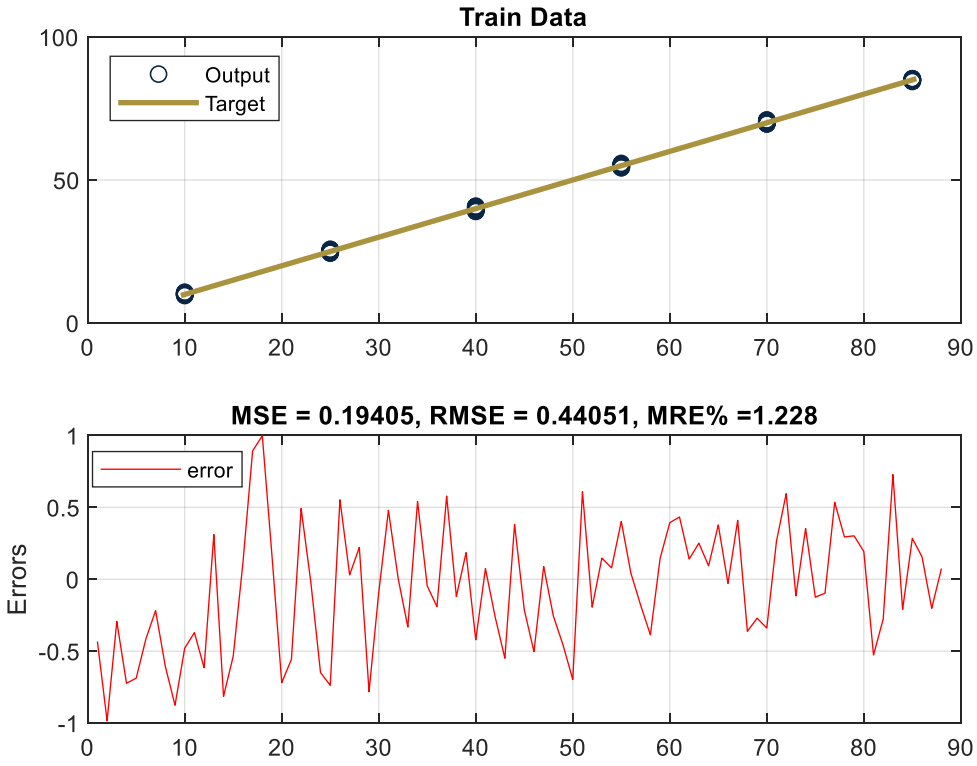

(**b**)

Figure 7. Designed network performance against (**a**) training and (**b**) testing data.

Wavelet transform is the technique used to extract the characteristics in this research. Advances to the fourth stage of wavelet transform led to the extraction of very suitable characteristics as neural network inputs. The comparison of this detection system with the others is shown in Table 2. It is clear that by extracting the convenient characteristics, the accuracy of the system can be outstandingly increased. In operating conditions, petroleum products are mixed in different types based on the pressure, temperature, and velocity of the products. Additionally, over time, the scale settles inside the oil pipes. In this study, in order for the proposed system to work properly in operating conditions, different conditions were simulated, including different flow regimes and different thicknesses of scales in different volume percentages. These simulations were considered primary data for system implementation. Finally, the detection of volume percentages independent of the type of flow regimes and the amount of scale inside the pipe with very high accuracy were considered as the advantages of this research. The study of three-phase flows with the method discussed in this article can be a good research topic for the subsequent study of researchers. The use of deep neural networks to determine the parameters of multiphase flows can also be evaluated for subsequent work. Requiring employees to use protective equipment when working with this device is a limitation of this research. The reason for this limitation is the inability to turn off the device and the device always being on.

Table 2. A comparison of the accuracy of the proposed detection system and previous studies.

Ref.	Extracted Features	Type of Neural Network	*MSE*		*RMSE*	
			Training	Testing	Training	Testing
[5]	Time-domain	MLP	0.21	0.036	0.46	0.6
[6]	Time-domain	GMDH	1.24	1.20	1.11	1.09
[7]	Lack of feature extraction	GMDH	7.34	4.92	2.71	2.21
[8]	Frequency-domain	MLP	0.17	0.67	0.42	0.82
[49]	Lack of feature extraction	MLP	17.05	9.85	4.13	3.14
[50]	Lack of feature extraction	MLP	2.56	2.56	1.6	1.6
[current study]	Wavelet feature	GMDH	0.19	0.12	0.44	0.35

6. Conclusions

Determining the volume percentage in scaled oil pipelines was the goal of this scrutiny. The Monte Carlo code became the basis for structural simulation in which the scale thickness was simulated at different volume percentages. The prementioned structure consists of a gamma energy source on one side of the pipe and a detector on the other side of the pipe. In this structure, all that is needed is radiation from the source to the detector. Radiation through the pipe is the main source of data collection. After collecting these data, the wavelet feature extraction technique was applied to access the high- and low-frequency information of the received signal. The average values of a4, d4, d3, d2, and d1 were given as inputs to the neural network to predict the volume percentage with an *RMSE* of less than 0.44. The superiority of this scrutiny over previous studies is the use of one detector. This reduction in the number of detectors is due to the wavelet feature extraction techniques and GMDH neural network. In addition to increasing the simplicity of the system, reducing the final manufacturing cost are advantages. According to the growing needs of the oil industry in the use of highly accurate and non-invasive devices to determine the parameters of multiphase flows, using the proposed methodology due to the high accuracy and low cost of the proposed system compared to previous ones is highly recommended.

Author Contributions: Formal analysis, A.K.A.; Funding acquisition, A.M.M.; Investigation, Z.A.K.; Methodology, A.M.M., A.A.A.-Q., H.H.A. and S.M.A.; Software, H.H.A., A.A.A.-Q. and A.M.M.; Supervision, E.N.; Visualization, E.E.-Z., E.N. and A.M.M.; Writing—original draft, S.M.A. and A.K.A. All authors have read and agreed to the published version of the manuscript.

Funding: The Deanship of Scientific Research at King Khalid University through General Research Project under grant number (GRP-20-41/2020). The authors acknowledge support from the German Research Foundation and the Open Access Publication Fund of the Thueringer Universitaets-und Landesbibliothek Jena Projekt-Nr. 433052568; the BMBF-Projekt 05P21SJFA2 Verbundprojekt 05P2021 (ErUM-FSP T05).

Institutional Review Board Statement: Not applicable.

Informed Consent Statement: Not applicable.

Data Availability Statement: Not applicable.

Conflicts of Interest: The authors declare no conflict of interest.

References

1. Snoek, C.W. A selection of new developments in multiphase flow measurement techniques. *Exp. Therm. Fluid Sci.* **1990**, *3*, 60–73. [CrossRef]
2. Basahel, A.; Sattari, M.A.; Taylan, O.; Nazemi, E. Application of Feature Extraction and Artificial Intelligence Techniques for Increasing the Accuracy of X-ray Radiation Based Two Phase Flow Meter. *Mathematics* **2021**, *9*, 1227. [CrossRef]
3. Taylan, O.; Sattari, M.A.; Essoussi, I.E.; Nazemi, E. Frequency Domain Feature Extraction Investigation to Increase the Accuracy of an Intelligent Nondestructive System for Volume Fraction and Regime Determination of Gas-Water-Oil Three-Phase Flows. *Mathematics* **2021**, *9*, 2091. [CrossRef]
4. Roshani, G.H.; Ali, P.J.; Mohammed, S.; Hanus, R.; Abdulkareem, L.; Alanezi, A.A.; Sattari, M.A.; Amiri, S.; Nazemi, E.; Eftekhari-Zadeh, E.; et al. Simulation Study of Utilizing X-ray Tube in Monitoring Systems of Liquid Petroleum Products. *Processes* **2021**, *9*, 828. [CrossRef]
5. Sattari, M.A.; Roshani, G.H.; Hanus, R.; Nazemi, E. Applicability of time-domain feature extraction methods and artificial intelligence in two-phase flow meters based on gamma-ray absorption technique. *Measurement* **2021**, *168*, 108474. [CrossRef]
6. Sattari, M.A.; Roshani, G.H.; Hanus, R. Improving the structure of two-phase flow meter using feature extraction and GMDH neural network. *Radiat. Phys. Chem.* **2020**, *171*, 108725. [CrossRef]
7. Roshani, M.; Sattari, M.A.; Ali, P.J.M.; Roshani, G.H.; Nazemi, B.; Corniani, E.; Nazemi, E. Application of GMDH neural network technique to improve measuring precision of a simplified photon attenuation based two-phase flowmeter. *Flow Meas. Instrum.* **2020**, *75*, 101804. [CrossRef]
8. Hosseini, S.; Roshani, G.H.; Setayeshi, S. Precise gamma based two-phase flow meter using frequency feature extraction and only one detector. *Flow Meas. Instrum.* **2020**, *72*, 101693. [CrossRef]
9. Hosseini, S.; Taylan, O.; Abusurrah, M.; Akilan, T.; Nazemi, E.; Eftekhari-Zadeh, E.; Bano, F.; Roshani, G.H. Application of Wavelet Feature Extraction and Artificial Neural Networks for Improving the Performance of Gas–Liquid Two-Phase Flow Meters Used in Oil and Petrochemical Industries. *Polymers* **2021**, *13*, 3647. [CrossRef]
10. Balubaid, M.; Sattari, M.A.; Taylan, O.; Bakhsh, A.A.; Nazami, E. Applications of Discrete Wavelet Transform for Feature Extraction to Increase the Accuracy of Monitoring Systems of Liquid Petroleum Products. *Mathematics* **2021**, *9*, 3215. [CrossRef]
11. Alamoudi, M.; Sattari, M.A.; Balubaid, M.; Eftekhari-Zadeh, E.; Nazemi, E.; Taylan, O.; Kalmoun, E.M. Application of Gamma Attenuation Technique and Artificial Intelligence to Detect Scale Thickness in Pipelines in Which Two-Phase Flows with Different Flow Regimes and Void Fractions Exist. *Symmetry* **2021**, *13*, 1198. [CrossRef]
12. Mayet, A.M.; Salama, A.S.; Alizadeh, S.M.; Nesic, S.; Guerrero, J.W.G.; Eftekhari-Zadeh, E.; Nazemi, E.; Iliyasu, A.M. Applying Data Mining and Artificial Intelligence Techniques for High Precision Measuring of the Two-Phase Flow's Characteristics Independent of the Pipe's Scale Layer. *Electronics* **2022**, *11*, 459. [CrossRef]
13. De Vuono, A.C.; Schlosser, P.A.; Kulacki, F.A.; Munshi, P. Design of an isotopic CT scanner for two phase flow measurements. *IEEE Trans. Nucl. Sci.* **1980**, *27*, 814–820. [CrossRef]
14. Dessimoz, A.-L.; Cavin, L.; Renken, A.; Kiwi-Minsker, L. Liquid–liquid two-phase flow patterns and mass transfer characteristics in rectangular glass microreactors. *Chem. Eng. Sci.* **2008**, *63*, 4035–4044. [CrossRef]
15. Lim, A.E.; Lam, Y.C. Vertical Squeezing Route Taylor Flow with Angled Microchannel Junctions. *Ind. Eng. Chem. Res.* **2021**, *60*, 14307–14317. [CrossRef]
16. Sharifi, S.; Aligoodarz, M.R.; Rahbari, A. Thermohydraulic performance of Al2O3-water nanofluid during single- phase flow and two-phase subcooled flow boiling. *Int. J. Therm. Sci.* **2022**, *179*, 107605. [CrossRef]
17. McKinney, G.W.; Dukee, J.W.; Hendricks, J.S.; James, M.R.; Pelowitz, D.B.; Water, L.S. *MCNP-X TM User's Manual*; Version 2.5.0. LA-CP-05e0369; Los Alamos National, Laboratory: Los Alamos, NM, USA, 2005.
18. Mandhane, J.M.; Gregory, G.A.; Aziz, K. A flow pattern map for gas—Liquid flow in horizontal pipes. *Int. J. Multiph. Flow* **1974**, *1*, 537–553. [CrossRef]
19. Lamari, M.L. An Experimental Investigation of Two-Phase (Air-water) Flow Regimes in a Horizontal Tube at Near Atmospheric Conditions. Ph.D. Thesis, Carleton University, Ottawa, ON, Canada, 2001.
20. Nazemi, E.; Roshani, G.H.; Feghhi, S.A.H.; Setayeshi, S.; Zadeh, E.E.; Fatehi, A. Optimization of a method for identifying the flow regime and measuring void fraction in a broad beam gamma-ray attenuation technique. *Int. J. Hydrog. Energy* **2016**, *41*, 7438–7444. [CrossRef]
21. Meric, I.; Johansen, G.A.; Mattingly, J.; Gardner, R.P. On the ill-conditioning of the multiphase flow measurement by prompt gamma-ray neutron activation analysis. *Radiat. Phys. Chem.* **2014**, *95*, 401–404. [CrossRef]
22. Holstad1, M.B.; Johansen, G.A. Produced water characterization by dual modality gamma-ray measurements. *Meas. Sci. Technol.* **2005**, *16*, 1007–1013. [CrossRef]
23. Daubechies, I. The wavelet transform, time-frequency localization and signal analysis. *IEEE Trans. Inf. Theory* **1990**, *36*, 961–1005. [CrossRef]
24. Soltani, S. On the use of the wavelet decomposition for time series prediction. *Neurocomputing* **2002**, *48*, 267–277. [CrossRef]
25. Ivakhnenko, A.G. Polynomial theory of complex systems. *IEEE Trans. Syst. Man Cybern.* **1971**, *SMC-1*, 364–378. [CrossRef]
26. Jahanshahi, A.; Sabzi, H.Z.; Lau, C.; Wong, D. GPU-NEST: Characterizing Energy Efficiency of Multi-GPU Inference Servers. *IEEE Comput. Archit. Lett.* **2020**, *19*, 139–142. [CrossRef]

27. Hayerikhiyavi, M.; Dimitrovski, A. A Practical Assessment of the Power Grid Inertia Constant Using PMUs. In Proceedings of the 2020 52nd North American Power Symposium (NAPS), Tempe, AZ, USA, 11–13 April 2021; pp. 1–5.
28. Arasteh, S.; Mahdavi, M.; Bideh, P.N.; Hosseini, S.; Chapnevis, A. Security Analysis of two Key Based Watermarking Schemes Based on QR Decomposition. In Proceedings of the Iranian Conference on Electrical Engineering (ICEE), Mashhad, Iran, 8–10 May 2018; pp. 1499–1504.
29. Pourbemany, J.; Zhu, Y.; Bettati, R. Breath to Pair (B2P): Respiration-Based Pairing Protocol for Wearable Devices. *arXiv* **2021**, arXiv:2107.11677.
30. Walid, W.; Awais, M.; Ahmed, A.; Masera, G.; Martina, M. Real-time implementation of fast discriminative scale space tracking algorithm. *J. Real-Time Image Process.* **2021**, *18*, 2347–2360. [CrossRef]
31. Moosaie, A.; Shekouhi, N.; Nouri, N.M.; Manhart, M. An algebraic closure model for the DNS of turbulent drag reduction by Brownian microfiber additives in a channel flow. *J. Non-Newton. Fluid Mech.* **2015**, *226*, 60–66. [CrossRef]
32. Rouhi, S.; Sadeqi, S.; Xiros, N.; Ioup, J. CFD Analysis of Filling Process for a Hydrogen Energy Storage System. In Proceedings of the American Society of Thermal and Fluids Engineers TFEC-2020-32066, New Orleans, LA, USA, 5–8 April 2020.
33. Sadeqi, S.; Xiros, N.; Rouhi, S.; Ioup, J.; Van Zwieten, J.; Sultan, C. In ASTFE Digital Library. In *Wavelet Transformation Analysis Applied to Incompressible Flow Field About A Solid Cylinder*; Begel House Inc.: Danbury, CT, USA, 2021.
34. Azhiri, R.B.; Jadidi, A.; Bideskan, A.S.; Dizadji, M.R. Ultrasonic nanocrystalline surface modification of low strength aluminum alloy: Trade-off between surface integrity and production rate aiming at desired fatigue life. *Int. J. Adv. Manuf. Technol.* **2021**, *113*, 1237–1251. [CrossRef]
35. Park, J.; Cho, Y.K.; Khodabandelu, A. Sensor-based safety performance assessment of individual construction workers. *Sensors* **2018**, *18*, 3897. [CrossRef]
36. Khodabandelu, A.; Choi, J.O.; Park, J.; Sanei, M. Developing a simulation model for lifting a modular house. In *Construction Research Congress 2020: Computer Applications*; American Society of Civil Engineers: Reston, VA, USA, 2020; pp. 145–152.
37. Arabi, M.; Beheshtitabar, E.; Ghadirifaraz, B.; Forjanizadeh, B. Optimum Locations for Intercity Bus Terminals with the AHP Approach–Case Study of the City of Esfahan. *Int. J. Environ. Ecol. Eng.* **2015**, *9*, 545–551.
38. Tomar, N.; Sadri, S.; Cowley, A.W., Jr.; Yang, C.; Quryshi, N.; Pannala, V.R.; Dash, R.K. A thermodynamically-constrained mathematical model for the kinetics and regulation of NADPH oxidase 2 complex-mediated electron transfer and superoxide production. *Free. Radic. Biol. Med.* **2019**, *134*, 581–597. [CrossRef] [PubMed]
39. Rashidisabet, H.; Thomas, P.J.; Ajilore, O.; Zulueta, J.; Moore, R.C.; Leow, A. A systems biology approach to the digital behaviorome. *Curr. Opin. Syst. Biol.* **2020**, *20*, 8–16. [CrossRef]
40. Heydarian, D.; Jolai, F. Simulation optimization of operator allocation problem with learning effects and server breakdown under uncertainty. *Prod. Manuf. Res.* **2018**, *6*, 396–415. [CrossRef]
41. Azadeh, A.; Heydarian, D.; Nemati, K.; Yazdanparast, R. Performance optimization of unique resilient human resource management system in a coal mine industry. *Int. J. Syst. Assur. Eng. Manag.* **2018**, *9*, 1178–1197. [CrossRef]
42. Mahmoudi, M. COVID Lessons: Was there any way to reduce the negative effect of COVID-19 on the United States economy? *arXiv* **2022**, arXiv:2201.00274.
43. Mahmoudi, M.; Ghaneei, H. Detection of structural regimes and analyzing the impact of crude oil market on Canadian stock market: Markov regime-switching approach. *Stud. Econ. Financ.* **2022**, *ahead of print*. [CrossRef]
44. Kharazmi, O.; Saadatinik, A.; Jahangard, S. Odd hyperbolic cosine exponential-exponential (OHC-EE) distribution. *Ann. Data Sci.* **2019**, *6*, 765–785. [CrossRef]
45. Rezaei, T.; Aslmarand, S.M.; Snyder, R.; Khajavi, B.; Alsing, P.M.; Fanto, M.; Miller, W.A. Experimental realization of Schumacher's information geometric Bell inequality. *Phys. Lett. A* **2021**, *405*, 127444. [CrossRef]
46. Gan, S.; Shao, S.; Chen, L.; Yu, L.; Jiang, L. Adapting Hidden Naive Bayes for Text Classification. *Mathematics* **2021**, *9*, 2378. [CrossRef]
47. Chen, S.; Zhang, Z.; Liu, L. Attribute Selecting in Tree-Augmented Naive Bayes by Cross Validation Risk Minimization. *Mathematics* **2021**, *9*, 2564. [CrossRef]
48. Yu, L.; Gan, S.; Chen, Y.; Luo, D. A Novel Hybrid Approach: Instance Weighted Hidden Naive Bayes. *Mathematics* **2021**, *9*, 2982. [CrossRef]
49. Roshani, M.; Ali, P.J.; Roshani, G.H.; Nazemi, B.; Corniani, E.; Phan, N.H.; Tran, H.N.; Nazemi, E. X-ray tube with artificial neural network model as a promising alternative for radioisotope source in radiation based two phase flowmeters. *Appl. Radiat. Isot.* **2020**, *164*, 109255. [CrossRef] [PubMed]
50. Peyvandi, R.G.; Rad, S.I. Application of artificial neural networks for the prediction of volume fraction using spectra of gamma rays backscattered by three-phase flows. *Eur. Phys. J. Plus.* **2017**, *132*, 511. [CrossRef]